Received: 1 February 2023 | Revised: 6 July 2023 | Accepted: 11 August 2023

DOI: 10.1002/mop.33872

RESEARCH ARTICLE

WILEY

An anisotropic broadband coding metasurface based on ultralight graphene-assembled film

Kaolin Luo[1] | **Haoran Zu**[1] | **Rongguo Song**[1] | **Yitong Xin**[1] | **Jiannan Guo**[1] | **Dong Ye**[1] | **Ming Xu**[1] | **Guan-Long Huang**[2] | **Daping He**[1]

[1]Hubei Engineering Research Center of RF-Microwave Technology and Application, School of Science, Wuhan University of Technology, Wuhan, China

[2]School of AI, Foshan University, Foshan, Guangdong, China

Correspondence
Rongguo Song and Daping He, Hubei Engineering Research Center of RF-Microwave Technology and Application, School of Science, Wuhan University of Technology, 430070 Wuhan, China.
Email: rongguo_song@whut.edu.cn and hedaping@whut.edu.cn

Funding information
National Natural Science Foundation of China, Grant/Award Numbers: 51672204, 51701146, 62001338; Fundamental Research Funds for the Central Universities, Grant/Award Numbers: 2020IB005, 205209016, 2019IB017

Abstract

As theoretical research further develops, coding metasurfaces have been widely studied and applied due to their uniqueness in digital characterization and sequence arrangement. In this work, based on highly conductive graphene-assembled film (GAF), an ultralight anisotropic broadband coding metasurface (ABCM) is proposed. The GAF ABCM consists of 16 units with specific phase responses and enables complete metal substitution. By arranging the unit cells in a specific order, the GAF ABCM realizes the functions of anomalous reflection, polarization conversion, and radar cross-section (RCS) reduction. Results validate that the GAF ABCM has a measured 10 dB normal incidence backward RCS reduction within the working frequency band of 7–18 GHz, which fully covers the X-band and Ku-band for radar application. Furthermore, due to the lightweight property of GAF, the density of the GAF ABCM is only 0.06 g/cm^3 (surface mass density of 0.038 g/cm^2). All results indicate that the lightweight GAF metasurface is promising in radar stealth and communication fields.

KEYWORDS

anisotropic, coding metasurface, graphene-assembled film, RCS reduction

1 | INTRODUCTION

As a new type of artificial electromagnetic material, electromagnetic metasurfaces provide new solutions and methods to manipulate electromagnetic waves flexibly.[1,2] Metasurfaces have good performance in modulating phase, amplitude, and polarization.[3–6] From the microwave to optical fields, various applications have been derived from metasurfaces, such as flat lens, anomalous reflections, electromagnetic stealth, holographic imaging, orbital angular momentum beam generation, dynamic beam-scanning, and dynamic beam-forming.[7–17] In 2014, the concept of "digital metamaterial" was first introduced by Della Giovampaola and Engheta.[18] Cui et al. also proposed the idea of coding metamaterial in the same year, effectively connecting code numbers with metasurface.[19] By arranging metasurface units in various coding orders, the electromagnetic wave can be freely and adaptably manipulated and controlled. In 2016, to achieve independent control of electromagnetic waves in the *x*- and *y*-directions, a dumbbell-shaped anisotropic coding metasurface was proposed by Liu et al.[20] The proposed anisotropic coding metasurface has extensively promoted the development of the multifunctional coding metasurface.

Among the various types of metasurfaces, the metasurface absorber, the coding metasurface, and the checkerboard surfaces all have outstanding performance in realizing radar cross-section (RCS) reduction and improving electromagnetic stealth performance.[21–25]

Nowadays, the majority of devices are required to achieve electromagnetic stealth in the X-band to Ka-band to ensure radar detection and wireless communication. However, there are several drawbacks existing in absorber metamaterials, like, ferromagnets and carbonyl iron nanocrystalline flakes, such as large thickness, high density, and processing challenge. The metals that are frequently employed in metamaterials also have significant flaws in corrosion resistance, weight, and thermal conductivity. Therefore, the realization of ultralight and superior physical properties of the new material-based metasurface is desired.

As a superior conductive material, graphene-assembled film (GAF) has the following advantages: lightweight, flexible, superior chemical stability, mechanical stability, and thermal conductivity. These characteristics are the reasons why GAF can be widely used in electromagnetic devices.[26–28] A lot of GAF RF devices have been proposed and have demonstrated that the GAF has a comparable loss level with copper when used in the radio-frequency band.[29–31] In our previous work, we designed an ultralight multilayer graphene-based metasurface for specular reflection suppression.[32] The metasurface can achieve dual reflection mechanisms including absorption and random diffusion within the same structure, which result in the backward reflection energy being significantly reduced in the ultrawideband range of 7.5–43 GHz. In addition, a graphene-based anisotropic filter that incorporates the characteristics of a phase gradient metasurface and an electromagnetic absorber was proposed, resulting in multiple beam behaviors and low reflection loss under orthogonal polarization.[33] However, the functions and the application scenarios of the above work are relatively limited, such as beam modulation and ultralight property.

In this paper, a 2-bit ultralight anisotropic broadband coding metasurface (ABCM) based on highly conductive GAF is proposed. When different polarization waves are incident, the GAF ABCM can achieve the functions of anomalous reflection, polarization conversion, and RCS reduction. The 10 dB RCS reduction band of the GAF ABCM is 7–18 GHz. All results indicate that the lightweight GAF metasurface is promising in radar stealth and wireless communication fields.

2 | DESIGN OF GAF ABCM UNIT

The mechanism of coding metasurface depends on the unit structure, and different functions can be realized by changing the arrangement order of the structural units on the metasurface. To satisfy the phase requirements, it usually ought to change the radiation phase of the unit by designing the structure of each coding metasurface unit. Taking a simple 1-bit coding metasurface as an example, each cell in the metasurface can be considered an individual. While the phase response of a reference unit represents the code number "0," another unit with a 180° phase difference can be set as code number "1." Therefore, after the normalization process, the unit cells with phase responses of 0° and 180° can be represented by the code numbers "0" and "1," respectively.

To achieve functional diversity, four fundamental units of 2-bit GAF metasurface, that is, "00," "01," "10," and "11," are designed in this work, as depicted in Figure 1A. The geometrical parameters for the 2-bit coding units are as follows: $w_1 = 0.5$ mm, $w_2 = 1$ mm, $w_3 = 0.7$ mm, $a_1 = 8.2$ mm, $a_2 = 7.1$ mm, $a_3 = 0.9$ mm, $p = 9$ mm, $t_1 = 6.3$ mm, and $t_2 = 0.025$ mm. Each of the four coding units displays normalized phase responses of 0°, 90°, 180°, and 270° when the x-polarized wave is incident vertically. The metasurface units comprise three layers, including the structural layer, the dielectric layer, and the reflective layer. The GAF used in this work was produced by applying a secondary high-temperature annealing to improve the conductivity: step1, preparing graphene oxide suspension; step2, roll-coating onto a polyethylene terephthalate; step3, evaporation drying; step4, thermally annealing in Ar atmosphere; step5, rolling and compressing; step6, annealing again under Ar atmosphere; step7, rolling at a pressure of 200 MPa.[29] The GAF with high conductivity of 1.1×10^6 S/m is used as the conductive material of the structural layer and the reflective layer. The polymethacrylimide (PMI) foam with a density of 0.05 g/cm^3 and a dielectric constant of 1.05 serves as the dielectric substrate material. In such design, the entire structure possesses lightness property.

The reflection coefficient and phase of the incident wave modulated by the metasurface are primarily taken into account in the electromagnetic simulation of the units. The simulation results of the GAF metasurface units are obtained by the commercial software CST Microwave Studio. When the x-polarized incident electromagnetic wave is vertically incident on the metasurface, the amplitude values and phase values of the four fundamental units "00," "01," "10," and "11" are obtained as shown in Figure 1B,C. The metasurface is close to total reflection, which satisfies the requirements of reflective coding metasurface. Meanwhile, the phase difference of the four GAF metasurface units is basically within the phase interval of $90° \pm 15°$ within 8–16 GHz and can be normalized to the phase values of 0°, 90°, 180°, and 270°.

On the basis of the 2-bit coding metasurface units, the 2-bit GAF ABCM is designed to make it more flexible to manipulate electromagnetic waves. Anisotropic

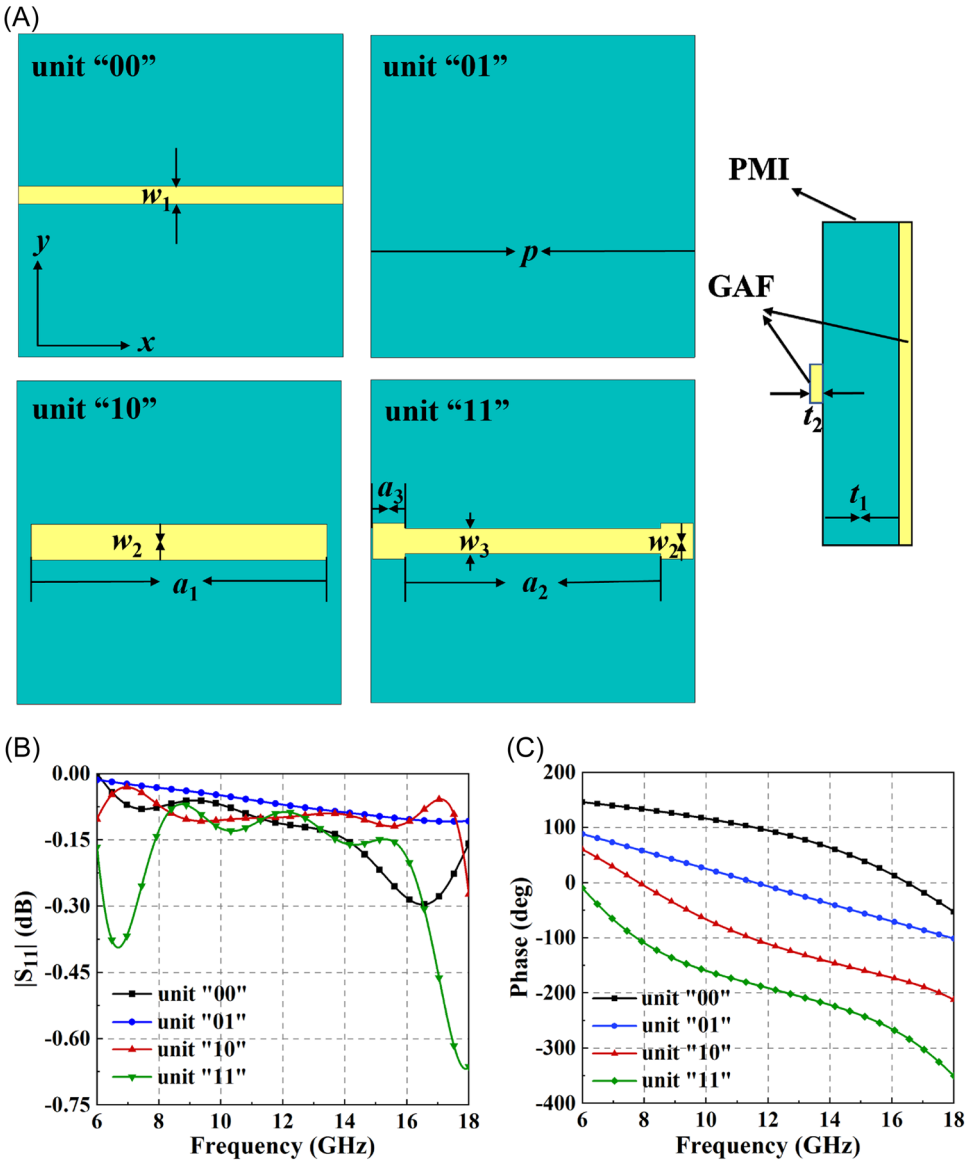

FIGURE 1 Schematic diagram of the two-dimensional unit structures and simulation results. (A) The pattern and the side view of the unit "00," "01," "10," and "11" (the yellow part is the GAF and the cyan part is the foam). (B) The simulation results of amplitude values and (C) phase values of the four units when the *x*-polarized wave is incident. GAF, graphene-assembled film; PMI, polymethacrylimide.

metasurface units can be formed by superimposing the original unit structure after 90° rotation of the 2-bit coding metasurface units. The 2-bit GAF ABCM needs 16 fundamental units since the coding units are designed to independently display four distinct states under *x*- and *y*-polarizations. Figure 2A displays the four isotropic unit structures that make up the 16 anisotropic fundamental units. The unit "10/11" represents the phase response of "10" in the *x*-direction and "11" in the *y*-direction, respectively. After a 90° rotation, the superposition of the units "10" and "11" results in the anisotropic unit structure "10/11." Figure 2B depicts the unit structure's phase response. The phase distribution is roughly consistent with that of "10" and "11" units in Figure 1C, and the phase difference is within $90° \pm 15°$ when *x*- and *y*-polarized waves are incidents. As a result, when the different polarization wave is incident, the structure's phase response exhibits a high degree of independence.

3 | MULTIFUNCTIONAL DESIGN OF GAF ABCM

On the basis of the aforementioned units, the design of the coding metasurface is carried out. Since the size of a single unit makes it difficult to reach the length of a wavelength, multiple unit cells need to be combined into

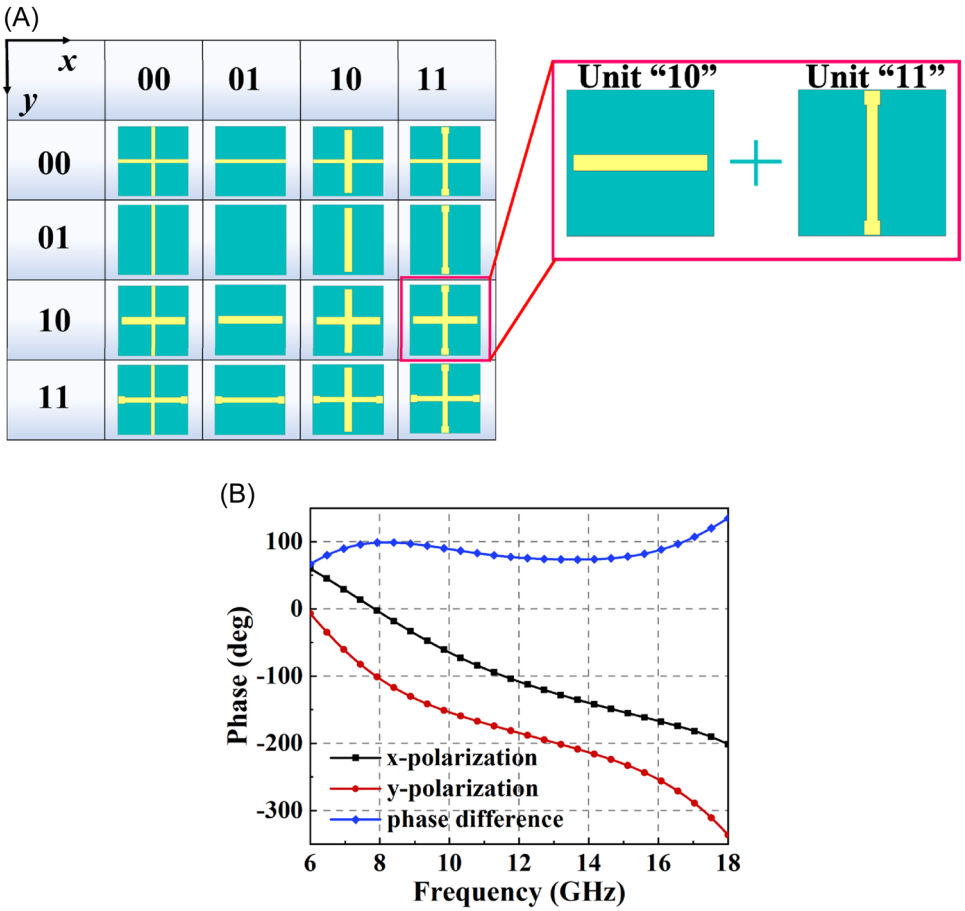

FIGURE 2 The 2-bit GAF ABCM units and their structural design instructions. (A) The structure of the 16 units of the 2-bit GAF ABCM and the formation process of the "10/11" unit structure. (B) Reflection phase and corresponding phase difference of anisotropic unit "10/11" when *x*- and *y*-polarized waves are incident. ABCM, anisotropic broadband coding metasurface; GAF, graphene-assembled film.

an array. In a metasurface, the units generally need to be expanded into a 3×3 array for the electromagnetic waves to be effectively reflected to free space.

To verify the ability of the coding metasurface to flexibly modulate the reflected beam, the same coding matrix (M_1) is utilized, as shown in Figure 3A,B. The reflected beam will be reflected in the free space at a certain deflection angle with the regular line. According to Snell's law and beam superposition theory, the magnitude of the reflection angle can be calculated by Equation (1). Where "λ" is the wavelength corresponding to the operating frequency in free space, and "Γ" is the gradient period length of the coding sequence.

$$\theta = \arcsin\left(\frac{\lambda}{\Gamma}\right). \tag{1}$$

At 10 GHz, it can be seen from Figure 3C that the metasurface is composed of 3×3 arrays with a beam deflection angle of 16° in the *y*–*o*–*z* plane. In comparison, the metasurface in Figure 3D is composed of 4×4 arrays with a deflection angle of 12° in the *y*–*o*–*z* plane, which is consistent with the result calculated by Equation (1). Figure 3E shows the two-dimensional simulation results of the two metasurfaces. It can be clearly seen from Figure 3E that the influence of different size arrays on the abnormal reflection angle. The coding matrix M_1 is arranged as follows:

$$M_1 = \begin{pmatrix} 00 & 01 & 10 & 11 \\ 00 & 01 & 10 & 11 \end{pmatrix}.$$

The GAF ABCM can also be used to design reflection-type quarter-wave plates that produce a circularly polarized wave deviating from the surface normal direction when the incident wave is polarized along 45° relative to the *x*-axis. By controlling the phase response difference of the coding unit in the *x*- and *y*-directions by 90°, the circularly polarized wave can be formed when the electromagnetic wave is incident. When lining up these coding units along a certain phase gradient in one direction, the circularly polarized wave is reflected

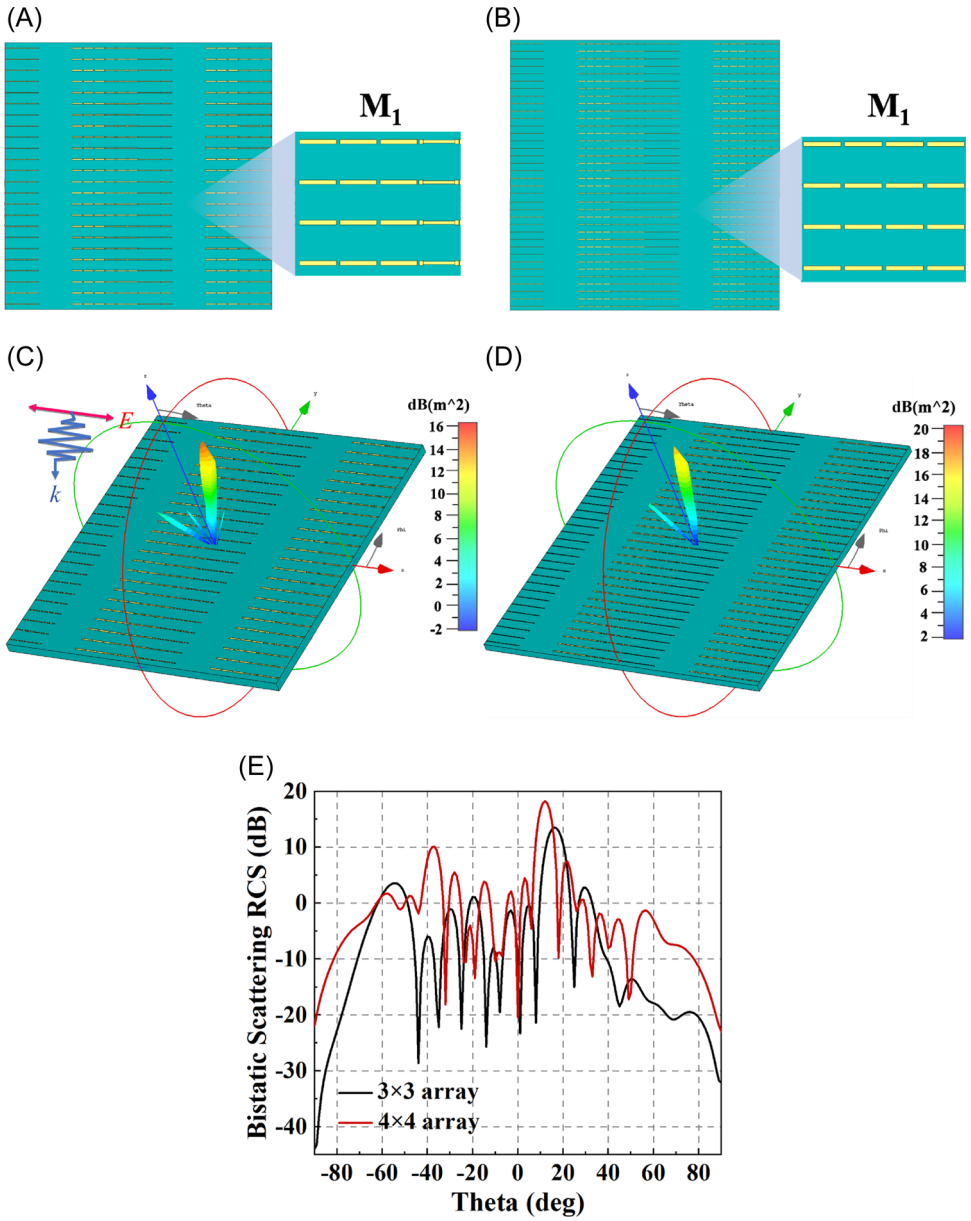

FIGURE 3 Structure and electromagnetic performance of the proposed metasurface with coding matrix M_1. (A) Pattern of metasurface composed of 3×3 arrays and (B) 4×4 arrays. (C–E) The 3D and 2D far-field scattering patterns of the metasurfaces in the sizes of 3×3 array and 4×4 array at 10 GHz, respectively.

toward a certain angle in free space. In this work, the coding matrix to achieve this function is M_2, and the metasurface pattern is shown in Figure 4A. The coding matrix M_2 is arranged as follows:

$$M_2 = \begin{pmatrix} 00/01 & 01/10 & 10/11 & 11/00 \\ 00/01 & 01/10 & 10/11 & 11/00 \end{pmatrix}.$$

The three-dimensional (3D) far-field diagram is shown in Figure 4B at 8, 10, 12, and 14 GHz. At 10 GHz, the reflection angle between the reflected beam and the normal line is 16°, which is consistent with the calculation result of Equation (1). As shown in Figure 4C, the beam reflection angle decreases as frequency rises, and gradually approaches 0°. To show the conversion ability of linear polarization to circular polarization, the abnormal reflection angle and the axial ratio at the maximum reflection angle of the metasurface within 6–18 GHz through simulation are obtained, as shown in Figure 4D. It can be seen from the black line in the figure that the reflection angle varies between 9° and 26°, and the variation rule is consistent with the rule

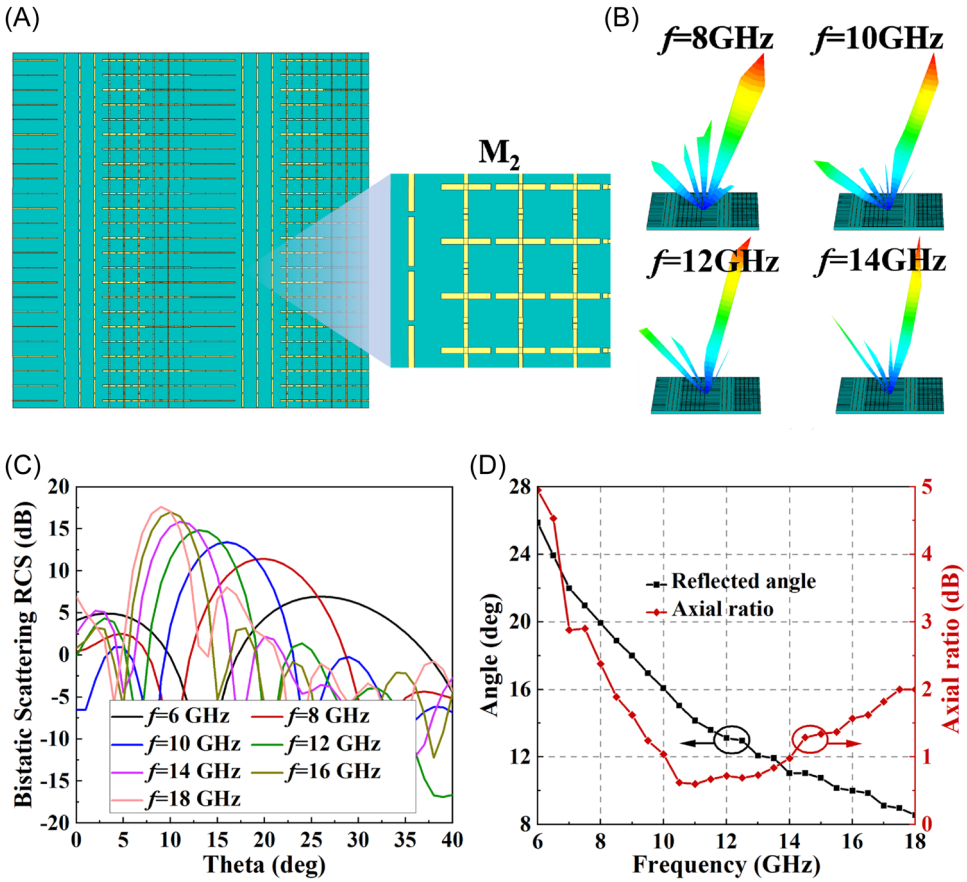

FIGURE 4 Structure and electromagnetic performance of the proposed metasurface with coding matric M_2. (A) Pattern of metasurface. (B) The 3D far-field scattering pattern of the metasurface at different frequencies. (C) Beam reflection angle and the bistatic scattering RCS at different frequencies. (D) Variation of the anomalous reflection angle (black line) and axial ratio (red line) of the metasurface over the frequency range 6–18 GHz. RCS, radar cross-section.

obtained by Equation (1). Moreover, it can be seen from the red line that the axial ratios are all less than 3 dB within 7–18 GHz. Therefore, it can be concluded that this reflection-type quarter-wave plate has excellent performance and can be used as an efficient circular polarizer.

When the units are arranged in the checkerboard form of M_3, the single incident beam is reflected off as four symmetrical beams about the normal, as shown in Figure 5A. The obtained far-field scattering pattern when the x-polarized wave is incident is shown in Figure 5B. RCS reduction is a significant application of coding metasurfaces. The pattern of the metasurface with coding matrix M_4 that conforms to random coding distribution is displayed in Figure 5C. Figure 5D shows the 3D far-field scattering pattern when the x-polarized wave is incident, the incident wave is reflected diffusely to all angles in free space. The arrangements of coding matrixes M_3, M_4, and M_5 are as follows:

$$M_3 = \begin{pmatrix} 01 & 10 \\ 00 & 11 \end{pmatrix},$$

$$M_4 = \begin{pmatrix} 00/01 & 01/01 & 11/01 & 10/01 & 10/01 & 01/01 & 00/01 & 11/01 \\ 11/01 & 10/01 & 00/01 & 01/01 & 11/01 & 00/01 & 01/01 & 10/01 \\ 10/01 & 11/01 & 01/01 & 00/01 & 01/01 & 10/01 & 11/01 & 00/01 \\ 01/01 & 00/01 & 10/01 & 11/01 & 00/01 & 11/01 & 10/01 & 01/01 \\ 00/01 & 11/01 & 10/01 & 01/01 & 10/01 & 11/01 & 01/01 & 00/01 \\ 01/01 & 10/01 & 11/01 & 00/01 & 01/01 & 00/01 & 10/01 & 11/01 \\ 11/01 & 00/01 & 01/01 & 10/01 & 00/01 & 01/01 & 11/01 & 10/01 \\ 10/01 & 01/01 & 00/01 & 11/01 & 11/01 & 10/01 & 00/01 & 01/01 \end{pmatrix},$$

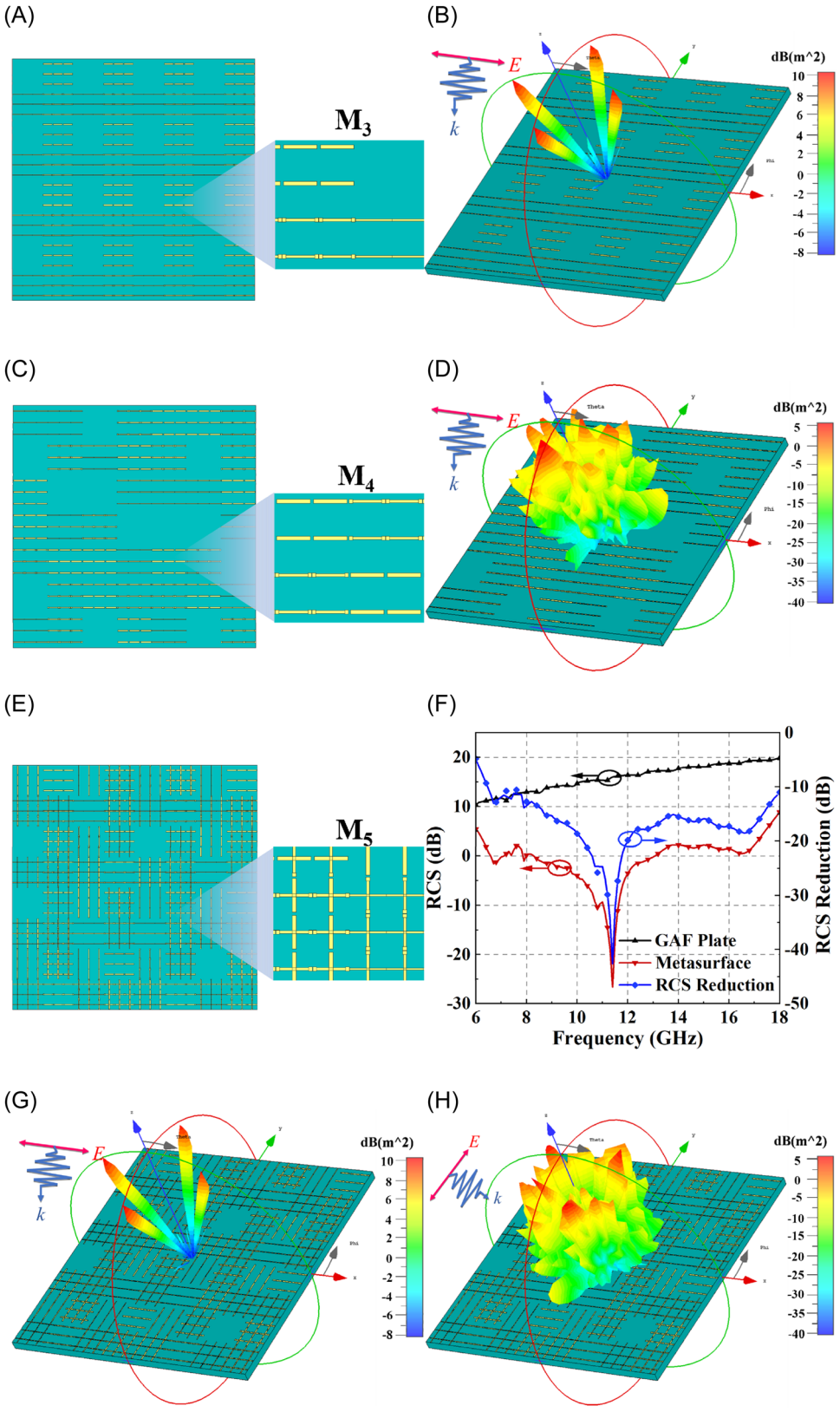

FIGURE 5 Structure and electromagnetic performance of the proposed metasurfaces with coding matrices M_3, M_4, and M_5. (A) Pattern of metasurface with coding matrix M_3 of checkerboard distribution. (B) The 3D far-field scattering pattern of the metasurface with coding matrix M_3. (C) Pattern of metasurface with coding matrix M_4 that conforms to a random coding arrangement. (D) The 3D far-field scattering pattern with random coding matrix M_4. (E) Pattern of GAF metasurface. (F) The RCS values of metasurface with random coding matrix M_5 and the GAF plate, and the RCS reduction performance while *y*-polarized waves incident. (G) The 3D far-field scattering pattern of the GAF metasurface with coding matrix M_5 when *x*- and (H) *y*-polarized waves incident. GAF, graphene-assembled film; RCS, radar cross-section.

$$M_5 = \begin{pmatrix} 00/01 & 01/10 & 11/01 & 10/10 & 10/01 & 01/10 & 00/01 & 11/10 \\ 11/00 & 10/11 & 00/00 & 01/11 & 11/00 & 00/11 & 01/00 & 10/11 \\ 10/01 & 11/10 & 01/01 & 00/10 & 01/01 & 10/10 & 11/01 & 00/10 \\ 01/00 & 00/11 & 10/00 & 11/11 & 00/00 & 11/11 & 10/00 & 01/11 \\ 00/01 & 11/10 & 10/01 & 01/10 & 10/01 & 11/10 & 01/01 & 00/10 \\ 01/00 & 10/11 & 11/00 & 00/11 & 01/00 & 00/11 & 10/00 & 11/11 \\ 11/01 & 00/10 & 01/01 & 10/10 & 00/01 & 01/10 & 11/01 & 10/10 \\ 10/00 & 01/11 & 00/00 & 11/11 & 11/00 & 10/11 & 00/00 & 01/11 \end{pmatrix}.$$

To test the anisotropy ability of the metasurface, the coding matrixes M_3 and M_4 are set in the x- and y-directions, respectively. Eventually, an anisotropic coding metasurface is formed with the coding matrix M_5 and the pattern of the metasurface is shown in Figure 5E. The metasurface is incident vertically by x- and y-polarized waves. Figure 5G,H shows that when the vertically polarized waves are incident, the metasurface performs the roles of RCS reduction and four symmetrically oriented beams reflection, respectively. The 3D far-field pattern demonstrates that when the incident polarization wave is independent, the results of the metasurface are consistent with the results above. When the y-polarized wave is incident, the RCS of the metasurface and GAF plate are calculated in Figure 5F. The orange and red lines compare the RCS of the metasurface to the RCS of the GAF plate, and the blue line demonstrates the RCS reduction. The figure shows that the RCS reduction values of the metasurface at 7–18 GHz are more than 10 dB, with a maximum RCS reduction of 42 dB.

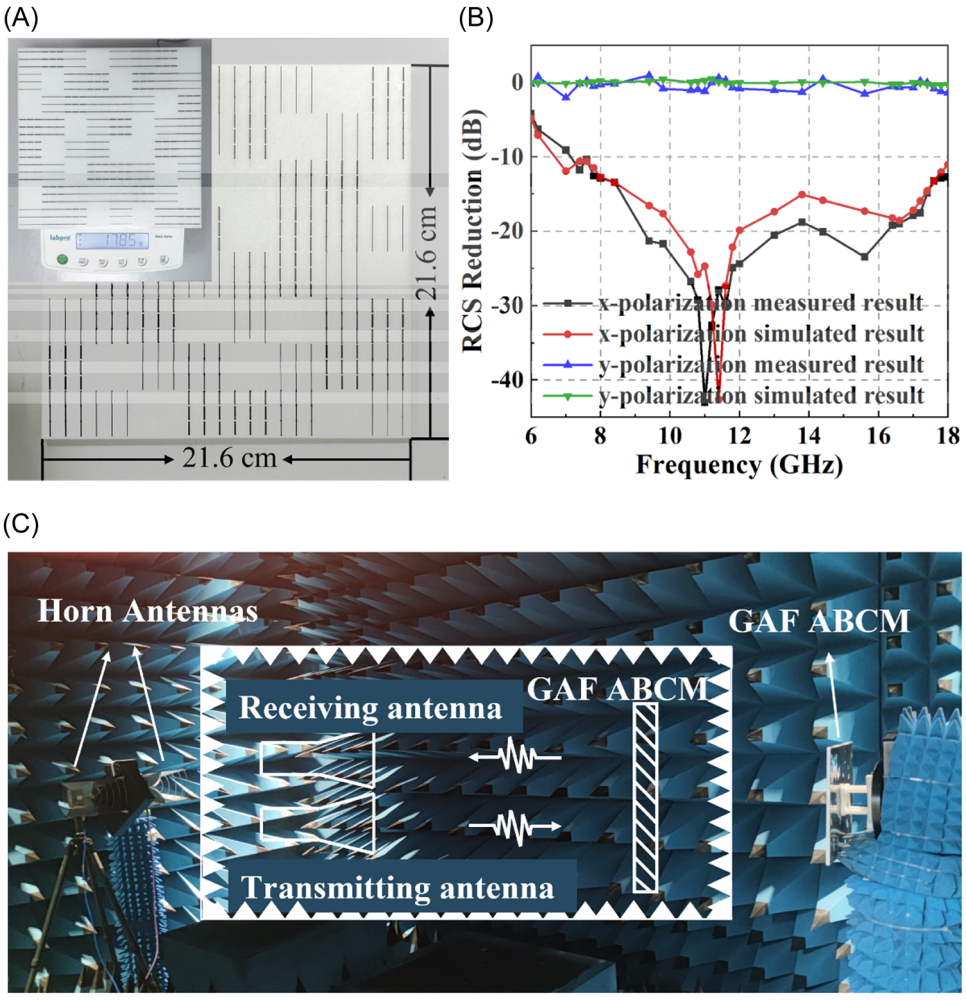

FIGURE 6 Prototype and measurement results of the proposed metasurface. (A) Photograph of the fabricated metasurface sample and the sample placed on an electronic balance. (B) Comparison diagram of simulation and measurement results. (C) The experimental and schematic diagram. ABCM, anisotropic broadband coding metasurface; GAF, graphene-assembled film; RCS, radar cross-section.

4 | MEASUREMENT OF GAF ABCM

A GAF ABCM sample with random coding sequences is processed for experimental verification. In the *x*-direction, the coding units are arranged in a random sequence, and in the *y*-direction, it can be regarded as a metasurface composed of "01" units. Similar to a metal plate, the incident wave will be reflected upon the metasurface when it is made up of identical coding units since their phase responses are consistent. The metasurface structure is created using a laser engraver on a highly conductive GAF, and the structure layer is then composited with the PMI foam material. A highly conductive GAF layer serves as the metasurface substrate and is highly effective at reflecting electromagnetic waves. The GAF metasurface, as shown in Figure 6A, which has a physical length of "21.6 cm × 21.6 cm," is made up of 24 × 24 units. To further demonstrate the lightweight characteristics of the metasurface more vividly, an electronic balance is used to weigh the fabricated sample, as shown in the upper left corner of Figure 6A. The corresponding calculated density is 0.06 g/cm^3 and the surface mass density is 0.038 g/cm^2. Figure 6C depicts the measurement environment of GAF ABCM and the schematic diagram. The metasurface as the sample to be tested is positioned at one end of the microwave anechoic chamber for far-field measurement.

As shown in Figure 6B, when the *x*-polarization wave is incident, the RCS reduction value is above 10 dB within 7–18 GHz. When the *y*-polarization wave is incident, the metasurface presents the function of total reflection, as shown by the blue and green lines in Figure 6B. Therefore, in the *x*- and *y*-directions, the metasurface achieves the electromagnetic stealth effect and total reflection, respectively. In addition, the test results agree substantially with the simulation results.

5 | CONCLUSIONS

By employing a highly conductive GAF and dielectric foam PMI, a lightweight 2-bit GAF ABCM is realized in this work. The GAF ABCM reacts differently to incident waves of various polarizations. In addition, by arranging the coding units, the coding metasurface can modulate the beam to achieve anomalous reflection and circular polarizer. Furthermore, the normal incidence backward RCS reduction function of GAF ABCM can be realized through random coding sequence optimization, which can accomplish more than 10 dB and up to 42 dB RCS reduction in the frequency range of 7–18 GHz. All results demonstrate that the GAF ABCM with outstanding multifunction and multifaceted features of ultralight and simple structure has a promising application prospect in radar detection and wireless communication.

ACKNOWLEDGMENTS

This work was financially supported by the National Natural Science Foundation of China Grant Nos. 51672204, 51701146, and 62001338, and the Fundamental Research Funds for the Central Universities Grant Nos. WUT: 2020IB005, 205209016, and 2019IB017.

DATA AVAILABILITY STATEMENT

The data that support the findings of this study are available from the corresponding author upon reasonable request.

ORCID

Guan-Long Huang http://orcid.org/0000-0003-2768-8266

Daping He http://orcid.org/0000-0002-0284-4990

REFERENCES

1. Veselago VG. Электродинамика веществ с одновременно отрицательными значениями ε и μ. *Usp Fiz Nauk*. 1967; 92(7):517-526.
2. Yu N, Capasso F. Flat optics with designer metasurfaces. *Nat Mater*. 2014;13(2):139-150.
3. Gao X, Han X, Cao WP, Li HO, Ma HF, Cui TJ. Ultrawideband and high-efficiency linear polarization converter based on double V-shaped metasurface. *IEEE Trans Antennas Propag*. 2015;63(8):3522-3530.
4. Guo WL, Wang GM, Luo XY, Chen K, Li HP, Feng Y. Dual-phase hybrid metasurface for independent amplitude and phase control of circularly polarized wave. *IEEE Trans Antennas Propag*. 2020;68(11):7705-7710.
5. Zheng B, Ren H, An S, et al. Tunable metasurface with dynamic amplitude and phase control. *IEEE Access*. 2021;9: 104522-104529.
6. Zhang K, Wang Y, Burokur SN, Wu Q. Generating dual-polarized vortex beam by detour phase: from phase gradient metasurfaces to metagratings. *IEEE Trans Microwave Theory Tech*. 2022;70(1):200-209.
7. Kwon DH. Lossless scalar metasurfaces for anomalous reflection based on efficient surface field optimization. *IEEE Antennas Wireless Propag Lett*. 2018;17(7):1149-1152.
8. Shi H, Li J, Zhang A, et al. Gradient metasurface with both polarization-controlled directional surface wave coupling and anomalous reflection. *IEEE Antennas Wireless Propag Lett*. 2015;14:104-107.
9. Chen W, Chen R, Zhou Y, Ma Y. A switchable metasurface between meta-lens and absorber. *IEEE Photonics Technol Lett*. 2019;31(14):1187-1190.
10. Shen C, Xu R, Sun J, Wang Z, Wei S. Metasurface-based holographic display with all-dielectric meta-axilens. *IEEE Photonics J*. 2021;13(5):1-5.
11. Liang L, Qi M, Yang J, et al. Anomalous terahertz reflection and scattering by flexible and conformal coding metamaterials. *Adv Opt Mater*. 2015;3(10):1311.

12. Ran Y, Shi L, Wu S, et al. Optically transparent ultrawideband electromagnetic stealth metasurface for microwave absorption and scattering. *IEEE Antennas Wireless Propag Lett*. 2022; 21(12):2412-2416.
13. Zhu L, Zhou W, Dong L, et al. Full space control of meta-holograms utilizing a bilayered patterned coding metasurface. *IEEE Antennas Wireless Propag Lett*. 2022;21(2):322-326.
14. Xing BB, Liu ZG, Lu WB, Chen H, Zhang QD. Wideband microwave absorber with dynamically tunable absorption based on graphene and random metasurface. *IEEE Antennas Wireless Propag Lett*. 2019;18(12):2602-2606.
15. Bai X, Zhang F, Sun L, et al. Time-modulated transmissive programmable metasurface for low sidelobe beam scanning. *Research*. 2022;9825903.
16. Bai X, Zhang F, Sun L, et al. Dynamic millimeter-wave OAM beam generation through programmable metasurface. *Nanophotonics*. 2022;11(7):1389-1399.
17. Bai X, Zhang F, Sun L, et al. Radiation-type programmable metasurface for direct manipulation of electromagnetic emission. *Laser Photonics Rev*. 2022;16(11):2200140.
18. Della Giovampaola C, Engheta N. Digital metamaterials. *Nat Mater*. 2014;13(12):1115-1121.
19. Cui TJ, Qi MQ, Wan X, Zhao J, Cheng Q. Coding metamaterials, digital metamaterials and programmable metamaterials. *Light: Sci Appl*. 2014;3(10):e218.
20. Liu S, Cui TJ, Xu Q, et al. Anisotropic coding metamaterials and their powerful manipulation of differently polarized terahertz waves. *Light: Sci Appl*. 2016;5(5):e16076.
21. Yoo M, Lim S. Polarization-independent and ultrawideband metamaterial absorber using a hexagonal artificial impedance surface and a resistor-capacitor layer. *IEEE Trans Antennas Propag*. 2014;62(5):2652-2658.
22. Shen Y, Pang Y, Wang J, Ma H, Pei Z, Qu S. Origami-inspired metamaterial absorbers for improving the larger-incident angle absorption. *J Phys D: Appl Phys*. 2015;48(44):445008-445014.
23. Han X, Xu H, Chang Y, et al. Multiple diffuse coding metasurface of independent polarization for RCS reduction. *IEEE Access*. 2020;8:162313-162321.
24. Malhat HA, Zainud-Deen SH, Shabayek NA. RCS reduction from conformal surfaces using plasma-based AMC arrays. *Plasmonics*. 2020;15(4):1025-1033.
25. Chen W, Balanis CA, Birtcher CR, Modi AY. Cylindrically curved checkerboard surfaces for radar cross-section reduction. *IEEE Antennas Wireless Propag Lett*. 2018;17(2):343-346.
26. Song R, Wang Q, Mao B, et al. Flexible graphite films with high conductivity for radio-frequency antennas. *Carbon*. 2018;130:164-169.
27. Song R, Mao B, Wang Z, et al. Comparison of copper and graphene-assembled films in 5G wireless communication and THz electromagnetic-interference shielding. *Proc Natl Acad Sci*. 2023;120(9):e2209807120.
28. Fang R, Song R, Zhao X, Wang Z, Qian W, He D. Compact and low-profile UWB antenna based on graphene-assembled films for wearable applications. *Sensors*. 2020;20(9):2552.
29. Song R, Jiang S, Hu Z, et al. Ultra-high conductive graphene assembled film for millimeter wave electromagnetic protection. *Sci Bull*. 2022;67(11):1122-1125.
30. Jiang S, Song R, Hu Z, Xin Y, Huang GL, He D. Millimeter wave phased array antenna based on highly conductive graphene-assembled film for 5G applications. *Carbon*. 2022;196:493-498.
31. Zu HR, Wu B, Zhang YH, Zhao YT, Song RG, He DP. Circularly polarized wearable antenna with low profile and low specific absorption rate using highly conductive graphene film. *IEEE Antennas Wireless Propag Lett*. 2020;19(12): 2354-2358.
32. Zhang C, Zhao J, Zhang BH, et al. Multilayered graphene-assisted broadband scattering suppression through an ultra-thin and ultralight metasurface. *ACS Appl Mater Interfaces*. 2021;13(6):7698-7704.
33. Zhang C, Long C, Yin S, et al. Graphene-based anisotropic polarization meta-filter. *Mater Des*. 2021;206:109768.

How to cite this article: Luo K, Zu H, Song R, et al. An anisotropic broadband coding metasurface based on ultralight graphene-assembled film. *Microw Opt Technol Lett*. 2023; 1-10. doi:10.1002/mop.33872